




# A Study on the Secondary Air Injection Method of the Combustor Considering Characteristics of Solid Refuse Fuels

J. S. Chae<sup>1</sup> · M. Y. Zhang<sup>1</sup> · S. J. Yang<sup>1</sup> · H. J. Rho<sup>1</sup> · J. W. Lee<sup>2</sup> · T. I. Ohm<sup>1</sup> 

Received: 18 January 2019 / Accepted: 22 July 2019 / Published online: 30 July 2019  
© Springer Nature B.V. 2019

## Abstract

This study used a numerical simulation method to design a grate-type combustion boiler for solid refuse fuel (SRF). First, proximate analysis, ultimate analysis, calorific value measurement, and combustion characteristic tests such as thermogravimetric analysis (TGA) and differential thermogravimetric analysis (DTG) were carried out to investigate the combustion characteristics of SRFs and municipal solid waste. To design an optimal SRF combustion steam boiler, the flow field, temperature distribution, chemical species concentration with varying secondary air injection angles and air ratios of the combustor need to be predicted. The secondary air injection angle affects fly ash generation on the grate, and the Cl compound in fly ash promotes high temperature corrosion in the superheater and heat exchanger of the boiler. The low heating values of two types of domestic waste are 13,062 kJ/kg and 14,402 kJ/kg, respectively, and that of fluff and densified SRFs are 19,552 kJ/kg and 29,014 kJ/kg, respectively. The concentration of Cl in densified SRF is 1.80 wt% and that of domestic waste and fluff SRF is 0.50 wt% or lower. The results of the TGA and DTG analyses reveal that the SRFs and domestic wastes complete their reactions at 500 °C or lower and at 540 °C, respectively. According to the numerical calculation results, it is optimal to inject the secondary air normally from the walls to suppress fly ash at the grate in the SRF combustor. Furthermore, an air ratio of 1.87 is recommended for stable combustion and prevention of high temperature corrosion on the walls of the heat exchanger tube.

---

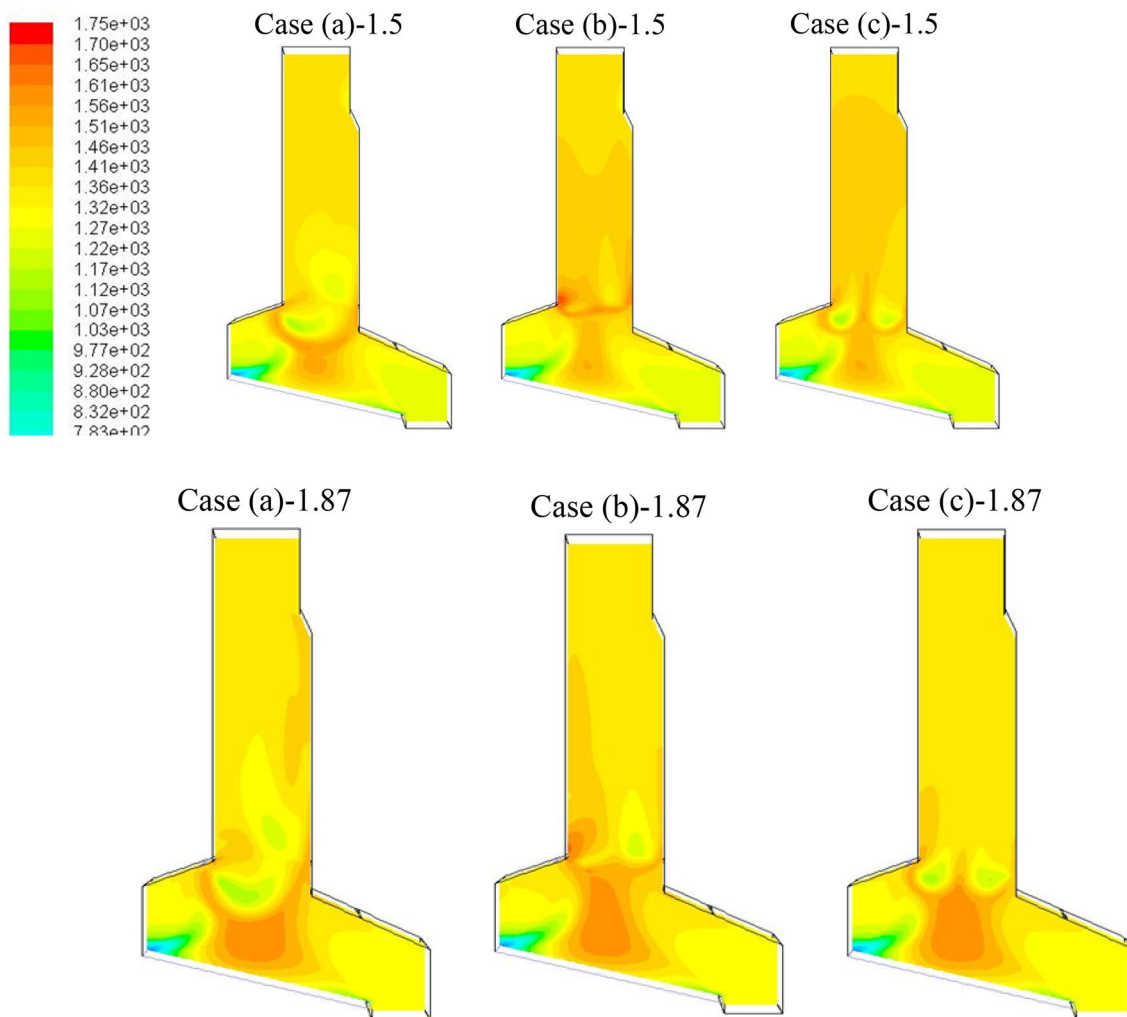
✉ T. I. Ohm  
tiohm1@hanbat.ac.kr

<sup>1</sup> Department of Civil & Environmental Engineering, Hanbat National University, Daejeon 34158, South Korea

<sup>2</sup> Department of Advanced Materials Engineering, Hanbat National University, Daejeon 34158, South Korea

## Graphic Abstract

Contours of temperature in combustor for SRF-B (°K)



**Keywords** Combustion steam boiler · Combustible waste · Numerical simulation · Solid refuse fuel (SRF) · Secondary air

## Statement of Novelty

To develop a large-scale combustion system for power generation using combustible solid waste, the fluff solid refuse fuel, densified solid refuse fuel and municipal solid waste were analyzed to test combustion characteristics. These combustible solid wastes were subjected to ultimate analysis, proximate analysis, heating value analysis, TGA and DTG. The computational analysis of the flow field, temperature profile, and concentration of chemical species were carried out according to the change of air ratio and the secondary air injection angle in grate-type combustion chamber using computational fluid dynamics (CFD). The CFD calculation results provide a useful design factor of the SRF combustor

for complete, stable combustion and prevention of the fly ash considering solid refuse fuel characteristics.

## Introduction

Korea has extremely insufficient energy resources, and most of the energy is imported. Hence, new and renewable energy resources must be developed, and their supply must be increased to secure stable energy. In recent years, the output of new and renewable energy has been increasing every year, and it comprises 4.7% of the energy in Korea based on data from 2015. Waste energy comprises 65% of new and

renewable energy; this is the component with the highest percentage, and its rate of increase is high.

The Korean government has played a leading role in reducing waste by incinerating combustible domestic waste for the last 20 years. Furthermore, extensive technological development has been made in efficiently recovering heat from incinerators owing to increasing prices of fossil fuels since 2008. Most domestic waste incinerators produce electricity and steam. However, the efficiency of these incinerators is 20% or lower for power generation and approximately 40% for heat utilization. As waste energy technologies can not only replace fossil fuels but also significantly reduce greenhouse gas emission, an increasing number of studies are being conducted on developing this particular technology. The Ministry of Environment in Korea is creating policies focused on the eco-friendly processing of combustible waste and the use of thermal energy for power generation from waste incinerators. The large amount of combustible waste to be converted into solid refuse fuel (SRF) to generate energy by revising the law in 2013. The previous four types of SRFs (refuse plastic fuel; RPF, refuse derived fuel; RDF, tire derived fuel; TDF, and wood chip fuel; WCF) were integrated and divided into two types (SRF and bio-SRF) and into fluff and densified products for manufacture and use.

The technologies for incineration, pyrolysis, and gasification have been commercialized for solid waste and biomass in EU and Japan. In Korea, the low quality of wastes and biomass were directly incinerated to recover energy in the past. However, in recent times, combustion techniques that use SRFs with improved fuel quality by preprocessing waste and biomass are being studied to increase energy recovery efficiency [1–4].

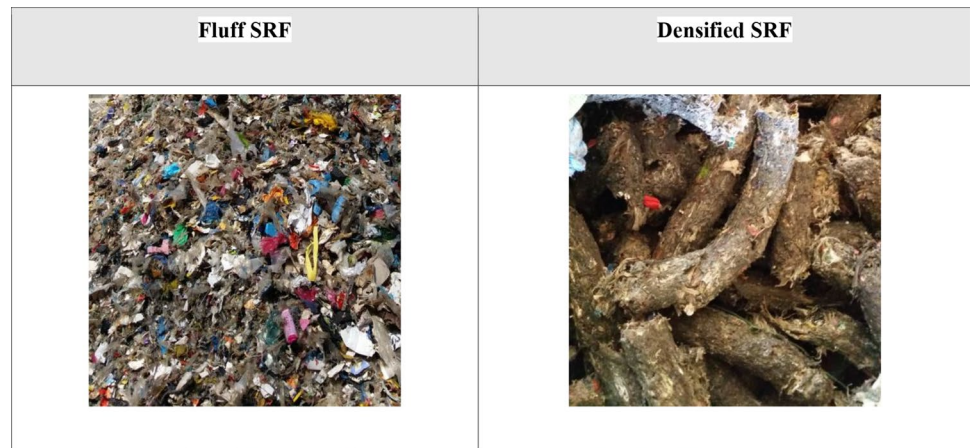
Applying SRFs to coal-fired power plants can cause unstable combustion and emission problems because of the different material properties. In addition, as more combustion boilers operate at increased steam temperatures to generate electric power during SRF incineration, the combustion efficiency degrades because of damage to equipment due to high temperature corrosion on the tube in superheaters, heat exchangers, and reheaters. To resolve these problems, numerous studies on slagging and fouling inside boilers, flame stability, and combustion characteristics have been carried out by several researchers [5–14].

In recent years, as fluff SRF production has expanded, SRF users are dissatisfied with environmental problems and low fuel quality in terms of low heating values. Additionally, there are increasing concerns on the differences in the qualities of SRFs. Therefore, it is extremely important to analyze the characteristics of SRFs to resolve the problems

associated with the combustion of SRFs or co-firing SRFs and coal. We analyzed the calorific values, ashes, and alkali-based Na, K, Ca, all of which cause corrosion. Moreover, large quantities of S, Cl components exist in fly ash that cause high temperature corrosion on the surface of heat exchanger. Therefore, the content of each material that causes high temperature corrosion must be analyzed and results must be incorporated in the steps of designing and constructing SRF combustion boilers [15–18]. Therefore, in order to prevent high temperature corrosion on the surface of heat exchanger of the SRF combustion system, it is essential to design technique to suppress fly ash generation. For this purpose, the computational analysis of the flow field and temperature profile by the secondary air injection in combustion chamber is important.

Usually, in municipal solid waste and SRF incinerator, the primary air is fed directly under the grate into the waste, and the secondary air is injected to unburned flue gas from the left and right side walls of the upper part of the grate. In this study, the design factors were calculated for secondary air supply, which is essential for future large-scale SRF combustion boiler system in power plants. To achieve this, this study performs proximate analysis, ultimate analysis, calorific value measurement, and combustion characteristic tests such as thermogravimetric analysis (TGA), and differential thermogravimetric analysis (DTG) for SRFs and domestic waste to evaluate basic pyrolysis and combustion characteristics [19]. The results are used as base data for designing and constructing a combustion steam boiler capable of predicting flow field, temperature distribution, and concentration values in a combustor. These factors are examined by varying the secondary air injection angles and air ratios on the upper part of the grate where the SRFs are burned by employing a numerical analysis approach. In the previous research, the temperature profile in combustion chamber was calculated when different air amount was injected by dividing the primary air into grate lengths [20]. However, studies on variation of the excess air ratio and secondary air injection angle were not found.

The numerical calculation is required for stable, complete SRF combustion and prevention of the fly ash considering solid refuse fuel characteristics. In this paper, the computational analysis of the flow field, temperature profile, and concentration of chemical species were carried out according to the change of air ratio and the secondary air injection angle in grate-type combustion chamber using computational fluid dynamics (CFD). Also in the SRF combustion system, when SRF contains S and Cl components, these components are attached to the surface of the heat exchanger by fly ash and melt, which causes high temperature corrosion.

**Fig. 1** Example of fluff SRF and densified SRF**Table 1** Result of proximate analysis of MSWs and SRFs

Components	Water (wt%)	Ash (wt%)	Volatile matter (wt%)	Fixed carbon (wt%)	Fuel ratio (FC/VM)	Low heating value (kJ/kg-wet)
MSW-A	18.4	31.5	37.9	12.2	0.32	13,063
MSW-B	18.9	26.4	36.5	18.2	0.50	14,403
SRF-A	8.9	3.2	79.3	8.6	0.11	29,015
SRF-B	17.0	12.6	62.3	8.1	0.15	19,552

**Table 2** Result of element analysis of combustibles for MSWs and SRFs

Components	C (wt%)	H (wt%)	N (wt%)	O (wt%)	S (wt%)	Cl (wt%)	Hg (ppm)	C/H
MSW-A	54.81	6.87	1.64	35.55	0.38	0.75	0.17	7.98
MSW-B	52.54	6.28	1.94	38.68	0.38	0.17	0.20	8.37
SRF-A	74.89	11.62	0.38	10.96	0.35	1.80	0.14	6.45
SRF-B	52.33	6.95	0.53	39.85	0.23	0.12	ND	7.53

## Samples of Solid Refuse Fuels

### Regulations of Solid Refuse Fuels in Korea

The waste used in SRF manufacturing materials comprises domestic waste (including waste furniture and excluding food), waste synthetic fiber, waste tires, waste synthetic resins, waste rubber, and bio-SRF manufacturing materials. The water contents of fluff and densified SRFs are 25.0 wt% and 10.0 wt% or lower, respectively. For these SRFs, the low heating value is 14,653 kJ/kg or higher, the ash content is 20 wt% or lower, the salt content is 2.0 wt% or lower, and the sulfur content is 0.6 wt% or lower. The concentration of Heavy metals (mercury, cadmium, lead, and arsenic) are 0.6, 5.0, 100, and 5.0 mg/kg or lower. The size is 50 × 50 mm or smaller.

The SRF manufacturing method is broadly divided into crushing and sorting processes. SRF is produced by performing the crushing/sorting processes on waste consisting

of vinyl, plastic, and paper that have high calorific values. These wastes are selected from the recycling products of major cities close to manufacturing factories. Densified SRF is manufactured from fluff SRF by using a densifying machine. Figure 1 shows the images of densified and fluff SRFs. In this study, samples were collected from two SRF manufacturing factories, and municipal solid waste (MSW) was collected from two locations to conduct experiments for comparing the combustion characteristics of the SRFs.

### Results of Proximate and Ultimate Analysis

In this study, the different wastes were used for the densified-SRF and fluff-SRF produced by the manufacturer.

The results of the proximate and element analyses for four types of samples are summarized in Tables 1 and 2, respectively. SRF-A (densified SRF) has the lowest water content because the water content is reduced owing to compression in the densifying process. The low heating values of MSW-A,

MSW-B, fluff SRF, and densified SRF are 13,063 kJ/kg, 14,403 kJ/kg, 29,015 kJ/kg, and 19,552 kJ/kg, respectively. Densified SRF has a higher low heating value compared with that of fluff SRF because its volatile matter content increases as water decreases in the manufacturing process.

The larger the C/H ratio, the greater the amount of soot that can be produced in the combustor. The C/H ratios of coal and gas are 10–30 and approximately 3, respectively. Generally, the fuel ratio of anthracite is 12 and that of lignite is 1 or lower [19]. The MSW and SRF samples have low fuel ratios of 1 or lower and low C/H ratios of 10 or lower compared with those of coal. This is because each of the four types of samples has low fixed carbon content and high volatile matter content, thereby reducing early ignition and burning time. Particularly, as the fuel ratios of the SRFs are lower than those of the MSWs, the SRF burning time is expected to be shorter than MSW burning time. Among the SRF components, fixed carbon is a carbon component that can be burned as indicated by proximate analysis results. In general, ash is classified as fly ash and bottom ash. The fly ash, which is a light material, is discharged along with the combustion gas, and the bottom ash, which is a heavy material, is discharged under the grate. A part of the fly ash may be melted at high temperature flue gas and attached to the heat exchanger, causing high temperature corrosion.

The Cl concentrations in MSW-A, MSW-B, SRF-A, and SRF-B are 0.75 wt%, 0.17 wt%, 1.80 wt%, and 0.12 wt%, respectively. The Cl concentrations in MSWs can vary depending on sample collection and location. The standard Cl concentration of the SRF is 2 wt% or lower, and an SRF with a Cl concentration of 0.5 wt% or lower is considered to be excellent. If the concentration of the Cl component is high, a large quantity of HCl gas is discharged. The Cl compound in fly ash promotes high temperature corrosion in the superheater and heat exchanger of boiler [21].

## Numerical Analysis Approach

### Mathematical Equations

The independent time equations of the numerical model are solved for conservation of mass, momentum, and energy for incompressible fluid [22]:

$$\nabla \cdot (\rho \vec{v}) = S_m; \tag{1}$$

$$\nabla \cdot (\rho \vec{v} \vec{v}) = -\nabla P + \nabla \cdot (\tau) + \rho \vec{g}; \tag{2}$$

$$\frac{\partial(\rho U_i E)}{\partial x_i} = \frac{\partial}{\partial x_i} \left[ \alpha_{eff} \frac{\partial T}{\partial x_i} - \sum h_j J_j + U_i (\tau_{ij})_{eff} \right] + S_h, \tag{3}$$

where

$$E = h - \frac{P}{h} + \frac{U_i^2}{2}; \tag{4}$$

$$h = \sum_i m_i h_i; \tag{5}$$

$$h_i = \int_{T_{ref}}^T C_{p_i} dT (T_{ref} = 298.15 \text{ K}); \tag{6}$$

$$S_h = - \sum \left( \frac{h_j^0}{M_j} + \int_{T_{ref}}^T C_{p_i} dT \right) R_i; \tag{7}$$

$$J_i = - \left( \rho D_{i,m} + \frac{\mu_t}{Sc_t} \right) \frac{\partial Y_i}{\partial x_i}; \tag{8}$$

$$(\tau_{ij})_{eff} = \mu_{eff} \left( \frac{U_j}{x_i} + \frac{U_i}{x_j} \right) - \frac{2}{3} \mu_{eff} \frac{U_i}{x_i} \delta_{ij}; \tag{9}$$

$$\alpha_{eff} = \alpha + \alpha_t. \tag{10}$$

The Eq. (1) represents conservation of mass, where  $\vec{v}$  is velocity,  $\rho$  is density and  $S_m$  is source of mass added to the continuous phase from the dispersed second phase and user-defined sources. In Eq. (1), it is assumed that the fuel is completely transformed into the gaseous phase at the very inlet of the grate-type combustor. Conservation of momentum is described by the Eq. (2), where  $p$  is the static pressure,  $\tau$  is the stress tensor, and  $\rho \vec{g}$  is the gravitational body force. The Eq. (3) represents the energy equation, where  $\alpha_{eff}$  is the effective conductivity,  $h$  is enthalpy, and  $J_j$  is the diffusion flux of species  $j$ .  $S_h$  includes the heat of chemical reaction, and any other volumetric heat sources [23].

### Turbulence Mode

The realizable  $\kappa - \epsilon$  model is a relatively recent development and has two important ways: (1) The realizable  $\kappa - \epsilon$  model contains a new formation for the turbulent viscosity. (2) A new transport equation for the dissipation rate,  $\epsilon$ , is derived from an exact equation for the transport of the mean-square vorticity fluctuation. The term “realizable” means that the model satisfies certain mathematical constraints on the normal stresses, consistent with the physics of turbulent flows. To understand

this, consider combining the Boussinesq relationship [23] and the eddy viscosity definition (11) to be the following expression for the normal Reynolds stress in an incompressible strained mean flow:

$$\mu_t = \rho C_\mu \frac{k^2}{\varepsilon} \quad (11)$$

$$\bar{u}^2 = \frac{2}{3}k - 2\nu_t \frac{\partial U}{\partial x} \quad (12)$$

Using  $\nu_t \equiv \mu_t/\rho$ , one obtains the result that the normal stress,  $\bar{u}^2$ , which by definition is a positive quantity, becomes negative, i.e., “non-realizable”, when the strain is large enough to satisfy [23],

$$\frac{k}{\varepsilon} \frac{\partial U}{\partial x} > \frac{1}{C_\mu} \approx 3.7 \quad (13)$$

In this study, based on the elemental analysis (Table 1) results of SRF-B, the gaseous compound formula of the  $C_aH_bO_cS_dN_e$  composition [24] was derived in this study. Furthermore the combustion chamber is assumed to be steady state. This study uses the realizable  $k$ – $\varepsilon$  model for turbulence proposed by Shih [23, 25]. This model uses a novel dissipation Eq. [23]. The  $k$  and  $\varepsilon$  are derived using Eqs. (14) and (15), respectively.

$$\frac{\partial}{\partial t}(\rho k) + \frac{\partial}{\partial x_i}(\rho k u_i) = \frac{\partial}{\partial x_i} \left[ \left( \mu + \frac{\mu_t}{\sigma} \right) \frac{\partial k}{\partial x_j} \right] + G_k + G_b - \rho \varepsilon - Y_M + S_k \quad (14)$$

$$\begin{aligned} \frac{\partial}{\partial t}(\rho \varepsilon) + \frac{\partial}{\partial x_j}(\rho \varepsilon u_j) &= \frac{\partial}{\partial x_i} \left[ \left( \mu + \frac{\mu_t}{\sigma} \right) \frac{\partial \varepsilon}{\partial x_j} \right] + \rho C_1 S_\varepsilon \\ &- \rho C_2 \frac{\varepsilon^2}{k + \sqrt{\nu \varepsilon}} + C_1 \varepsilon \frac{\varepsilon}{k} C_3 \varepsilon G_b + S_\varepsilon \end{aligned} \quad (15)$$

$C_1$  in Eq. (15) is given by

$$C_1 = \max \left[ 0.43, \frac{n}{n+5} \right], \quad \eta = S_\varepsilon \frac{k}{\varepsilon}, \quad S = \sqrt{2S_{ii}S_{ii}} \quad (16)$$

In these equations,  $G_k$  represents the generation of turbulence kinetic energy due to the mean velocity gradients,  $G_b$  is the generation of turbulence kinetic energy due to buoyancy.  $Y_M$  represents the contribution of the fluctuating dilatation in compressible turbulence to the overall dissipation rate.  $C_2$  and  $C_1$  are constants.  $\sigma_k$  and  $\sigma_\varepsilon$  are the turbulent Prandtl numbers for  $k$  and  $\varepsilon$ , respectively.  $S_k$  and  $S_\varepsilon$  are user-defined source terms [23].

## Combustion Chamber and Boundary Conditions

The shape of the grate-type combustion steam boiler to generate power for SRF-B was modeled for the numerical analysis, and it is shown in Fig. 2. The combustion chamber

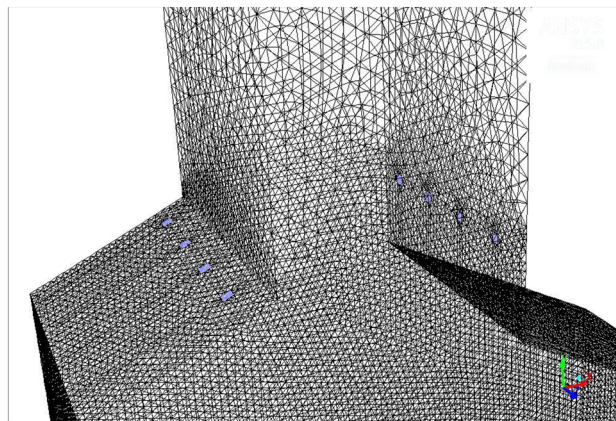


Fig. 2 Mesh structure and the secondary air injection point

Table 3 Inlet boundary conditions of SRF-B and air

	SRF (CaHbOcSdNe)	Air	
		Primary air	Secondary air
Feed rate	500 kg/h	3408.3 kg/h	1460.7 kg/h
Temperature	293 K	293 K	293 K

with SRF-B capacity of 500 kg/h is 4.92 m in width, 2.0 m in depth and 10.0 m in height and the grate size is 2.0 m in depth and 3.92 m in width. In case a grate-type combustion boiler is used in the analysis, drying, pyrolysis, char burning, and post combustion processes are performed on the grate to which the SRF is supplied [24].

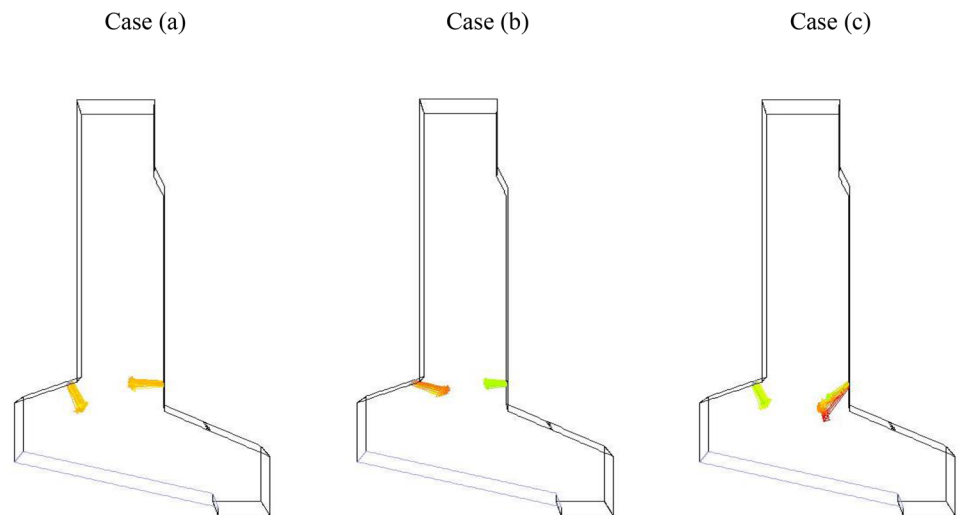
The Tgrid mesh type is applied to the calculation domain. For verifying the number of grids, the number of cells was calculated from 500,000 to 1,500,000, and the optimal number of cells was determined to be 1,026,553. In addition, the size of the mesh varies from 46 to 85 mm. As the SRF-B supplied to the combustor has non-uniform composition depending on the actual supply time, the analysis is carried out by considering the average values derived through the proximate and element analyses of the SRF-B (Tables 1, 2). To verify the adequacy of the mesh and model, the flue gas temperature at the outlet of the combustion chamber was theoretically calculated.

Table 3 shows the inlet boundary conditions of SRF-B and air for numerical calculation. The commercial code used in this study is FLUENT version 15 [23].

A dense grid was created on the grate of the combustor where flames are formed and the secondary air injection nozzle to achieve high accurate numerical calculation. A coarse grid was additionally created on the upper part of the combustion boiler to reduce calculation time. Four the secondary air inlets having the same area were arranged on the left and right sides of the boiler wall. Usefulness in design

**Table 4** Reaction parameters of Eqs. (17) and (18)

Reaction equations	(17)						(18)		
Reactants and products	Reactants		Products				Reactants		Product
Component	SRF	O <sub>2</sub>	CO	H <sub>2</sub> O	SO <sub>2</sub>	N <sub>2</sub>	CO	O <sub>2</sub>	CO <sub>2</sub>
Stoichiometric coefficient	1	0.735	1	0.836	0.0008	0.015	1	0.5	1
Rate exponent	0.5	1.25	0	0	0	0	0.5	1.25	0
Pre-exponential factor	4e+11						1.3e+11		
Activation energy	1.256e+08 J/kmol						1.256e+08 J/kmol		
Temperature exponent	0						0		
Mixing rate constants A and B	A : 4, B : 0.5						A : 4, B : 0.5		

**Fig. 3** The velocity vectors of the secondary air injection

and manufacture was verified by analyzing the temperature characteristics inside the boiler and exhaust gas characteristics by changing the secondary air injection angles.

### Combustion Model

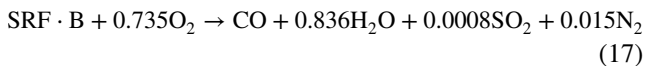
The eddy-dissipation model assumes that reactions are fast and that the system is purely mixing limited. When that is not the case, it can be combined with finite-rate chemistry. In that case, the kinetic rate is calculated in addition to the reaction rate predicted by the eddy-dissipation model. The

slowest reaction rate is then used: if turbulence is low, mixing is slow and this will limit the reaction rate. The reaction rate will be limited if turbulence is high but the kinetic rate is low. This model can be used for various system, but with the following caveats: the model constants A and B need to be empirically adjusted for each reaction in each system. Default values of 4.0 and 0.5 were determined for one and two-step combustion processes, respectively. In this study, SRF-B is assumed to be the combustible compound of  $C_aH_bO_cS_dN_e$  having a gaseous phase [24]. The finite-rate/eddy-dissipation model was selected for chemical reaction.

**Table 5** Excess air ratios and the secondary air injection angles

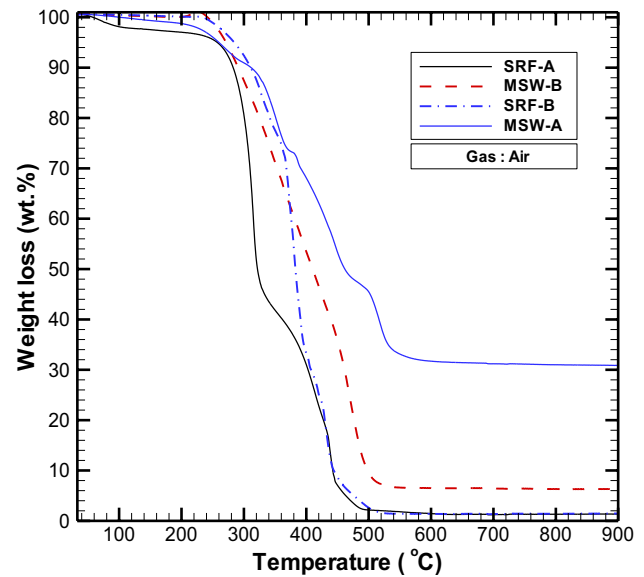
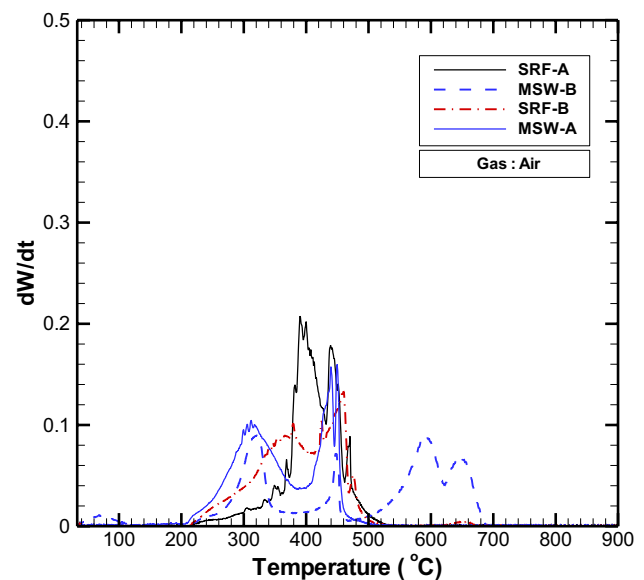
Case no.	Air ratio	Injection angle (°)	
		Left wall	Right wall
Case (a)-1.5	1.5	Normal (90)	Normal (90)
Case (b)-1.5	1.5	Counterclockwise (45)	Normal (90)
Case (c)-1.5	1.5	Normal (90)	Counterclockwise (45)
Case (a)-1.87	1.87	Normal (90)	Normal (90)
Case (b)-1.87	1.87	Counterclockwise (45)	Normal (90)
Case (c)-1.87	1.87	Normal (90)	Counterclockwise (45)

This model is widely used in turbulence combustion models [22, 23, 26]. The combustion process was analyzed by a two-step reaction between oxidizer and SRF-B. The reaction mechanism is given in Eqs. (17) and (18). Table 4 lists the reaction parameters used for the numerical analysis.



In calculation of radiation heat transfer, the ‘Discrete ordinates’ radiation model is applied. This model spans the entire range of optical thicknesses, and allows us to solve problems from surface-to-surface radiation to participating radiation in combustion [23]. The secondary air injection angles in the combustion chamber are illustrated in Fig. 3. In case (a), the secondary air is injected normal (90° on the left wall and 90° on the right wall) to the left and right walls. In case (b), secondary air is injected at 45° counterclockwise to the left wall and 90° to the right wall. In case (c), secondary air is injected at 90° to the left and 45° counterclockwise to the right wall.

A velocity-inlet condition was applied to the primary air inlet at the bottom part of the grate-type combustor, and a mass-inlet condition was applied to the secondary air inlet to analyze the changes in the amounts of injection. The conditions for the numerical calculation performed are listed in Table 5.

**Fig. 4** TGA curves of MSWs and SRFs (heating rate: 10 °C/min, carrier gas: air)**Fig. 5** DTG curves of MSWs and SRFs (heating rate: 10 °C/min, carrier gas: air)



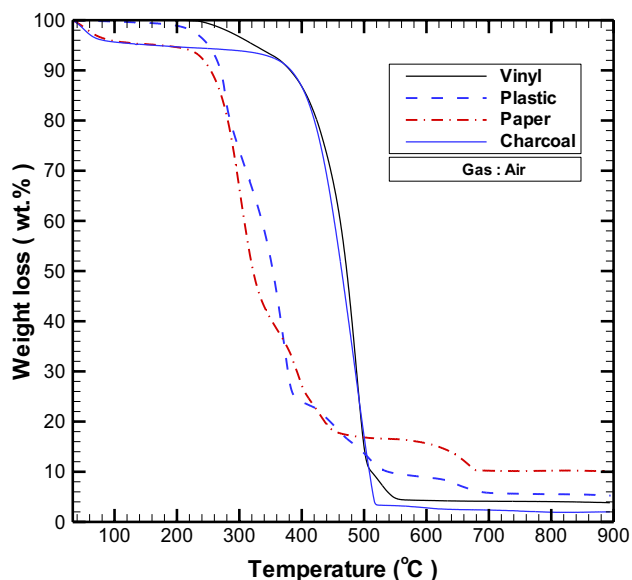


**Fig. 6** TGA curves of SRF-B components (heating rate: 10 °C/min, carrier gas: air)

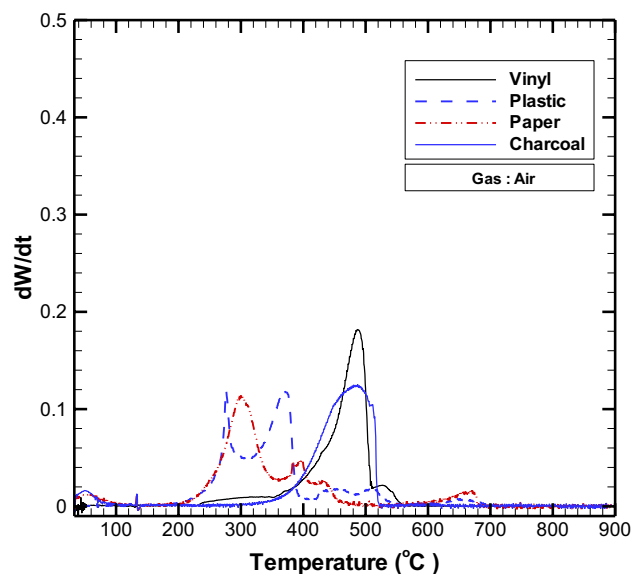


**Fig. 7** DTG curves of SRF-B components (heating rate: 10 °C/min, carrier gas: air)

## Results and Discussion

### Results of the TGA and the DTG

The TGA is widely used for studying the thermal stability of the solid fuels and state change processes by heating. The physical and chemical changes in a sample can be understood by observing the changes in weight of the sample caused by heating. Then, they are used to understand the various phenomena that result from heating. In addition, the changes in combustion rate can be acquired for each temperature zone by obtaining DTG graphs.

The TGA has a basic mechanism consisting of three steps, i.e., drying, devolatilization, and char burning. Figure 4 shows the TGA results used to identify the combustion characteristics of domestic waste and SRFs. Air was used as the carrier gas, and its temperature was increased from 30 to 900 °C at a heating rate of 10 °C/min. The MSWs and SRF-B with high water contents lose their weights at approximately 100 °C and discharge and combust initial volatile matter, carbon, and residual volatile matter contents between 250 and 550 °C. Generally, the weight of surface moisture is

reduced until 150 °C and devolatilization reactions occur from 200 °C. The weight rapidly decreases between 200 and 500 °C because depolymerization reactions occur and volatile matters are combusted. After 540 °C, the decomposition of the SRFs and MSWs is almost completed and weight changes slightly.

The DTG curves are shown in Fig. 5. The curves show the weight loss rates of the samples as functions of temperature and enable one to more clearly determine combustion characteristics. A low peak in the DTG curve results in a small change in weight loss. The higher the peak, the larger the weight loss per unit time at the corresponding temperature. The results of the DTG curve reveal that the peak shapes of the MSWs and SRFs are different. The fluff and densified SRFs with high vinyl and plastic contents have different peak shapes. When oxygen is supplied as a reaction gas to observe the pyrolysis reactions of the samples, the MSWs, which have lower volatile matter and higher fixed carbon contents compared to the SRFs, have two peaks at 340 °C and 460 °C, and the SRFs have a peak at 440–460 °C. This is because the MSWs have high ash contents with mixed combustible and noncombustible components, and the SRFs

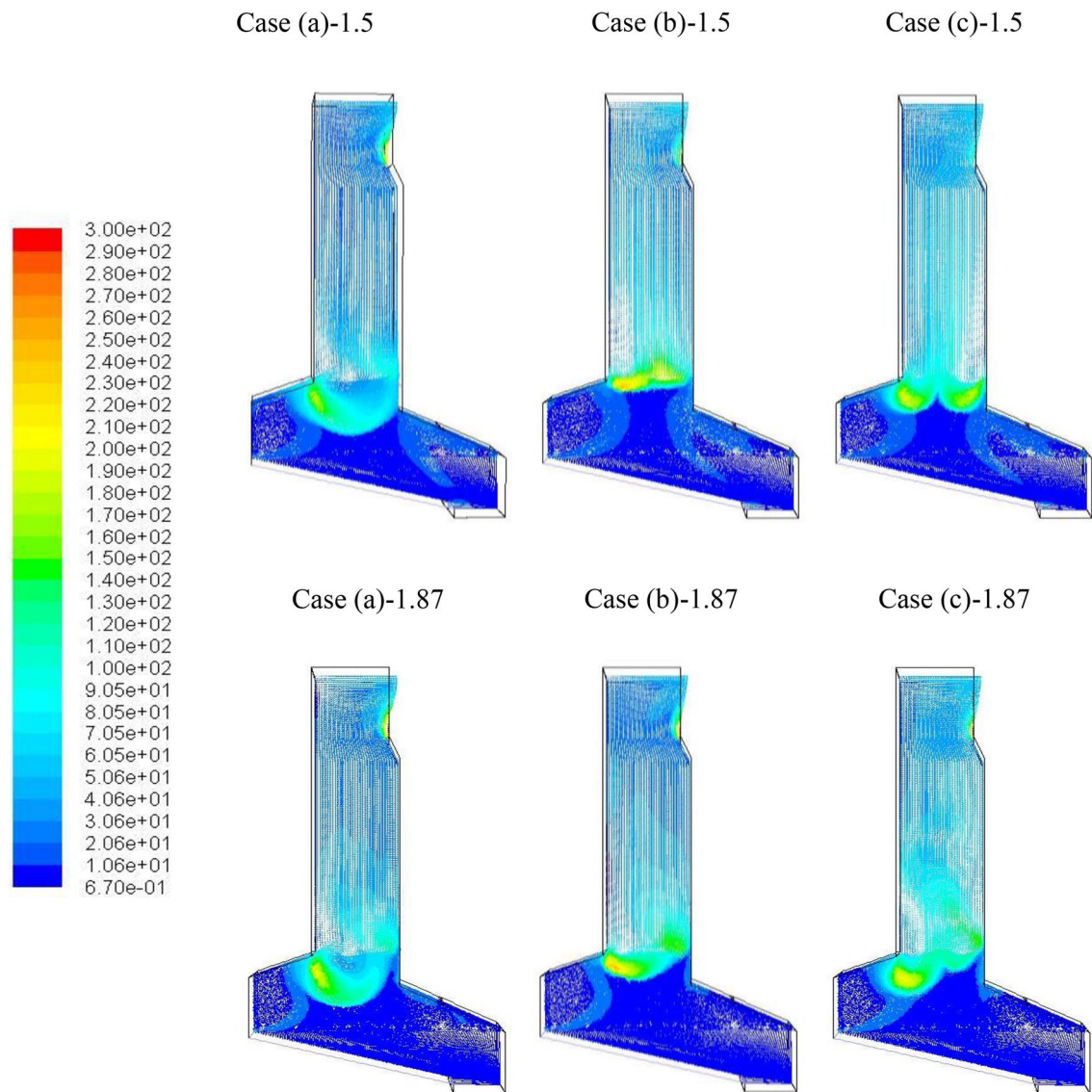


**Fig. 8** Vectors of turbulent intensity in combustor for SRF-B (%)

are produced by selecting combustible components only. The weights of the SRFs change slightly after 500 °C, and all reactions are completed before 500 °C.

The TGA results of SRF-B by components are shown in Fig. 6. The carrier gas is air, and its temperature is increased from 30 to 900 °C at a heating rate of 10 °C/min. The components for the TGA are plastic, paper, vinyl, and other unclassified components. Additionally, the TGA

of charcoal is shown for comparison. Plastic, paper, and vinyl complete their reactions at 500 °C, 500 °C, and 540 °C, respectively, and show slight changes in weight loss afterwards.

In SRF-B, the highest content is that of vinyl, followed by that of plastic and paper. As the reaction of vinyl is completed at the highest temperature and its content is the highest, it is expected to have the largest effect on

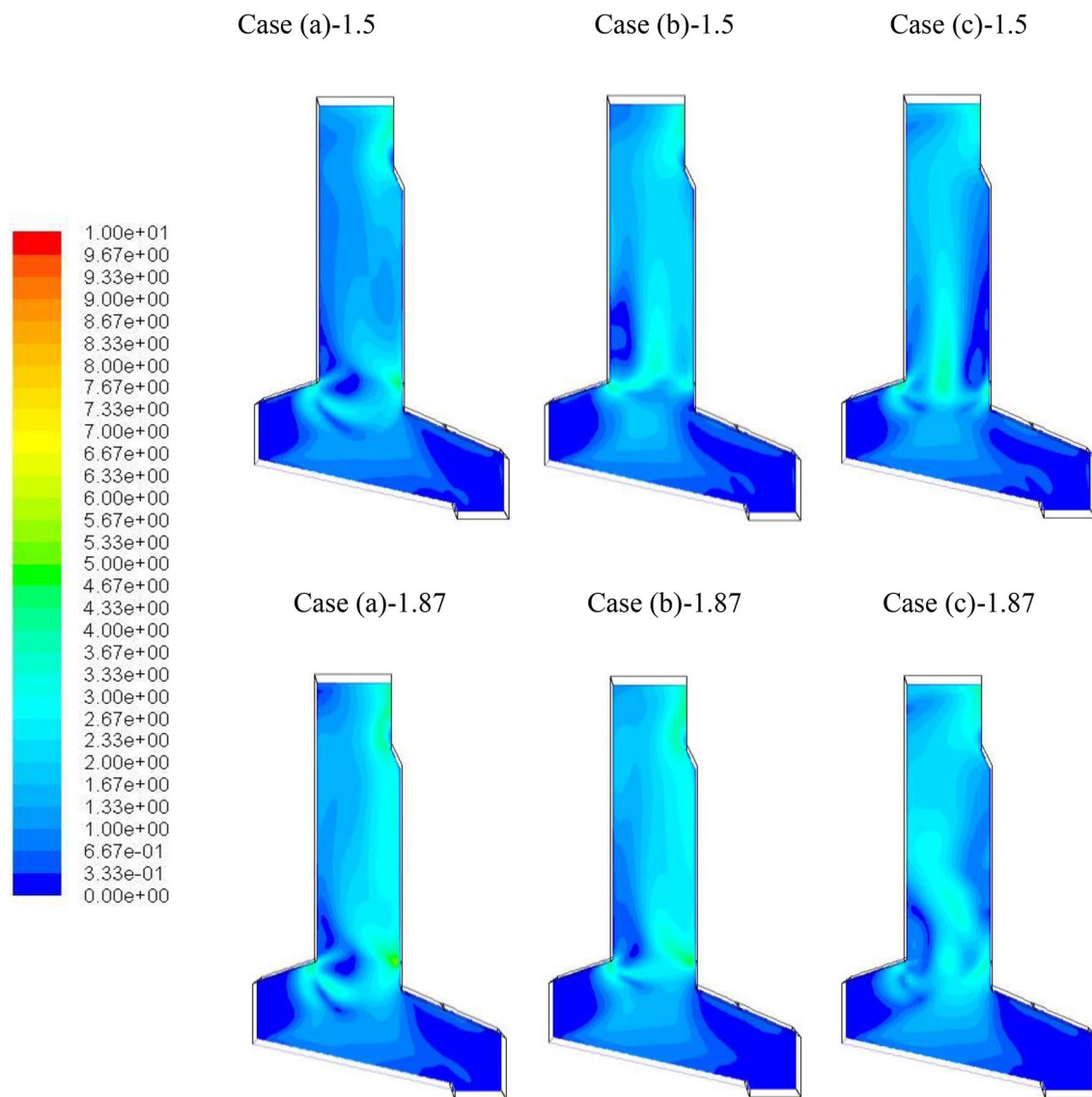


**Fig. 9** Contours of velocity magnitude in combustor for SRF-B (m/s)

the combustion rate and characteristics of SRF-B. As the combustion characteristics of an SRF can be determined if the contents of the produced SRF are analyzed by component, the combustion characteristics may change in accordance with the mixing ratio of each component. The DTG curves of SRF-B are shown in Fig. 7. Vinyl, charcoal, and plastic have only one weight loss change rate peak with varying temperature because they are single materials. Vinyl exhibits the highest weight loss at the highest temperature.

## Results of Numerical Analysis

### Turbulent Intensity and Velocity Distribution in Combustion Chamber

The vectors of turbulent intensity in the combustion chamber for SRF-B with varying air ratios and secondary air injection angles are shown in Fig. 8. In CFD, the turbulence intensity, is defined as the ratio of the root-mean-square of the velocity fluctuations, to the mean flow velocity. Even though the air

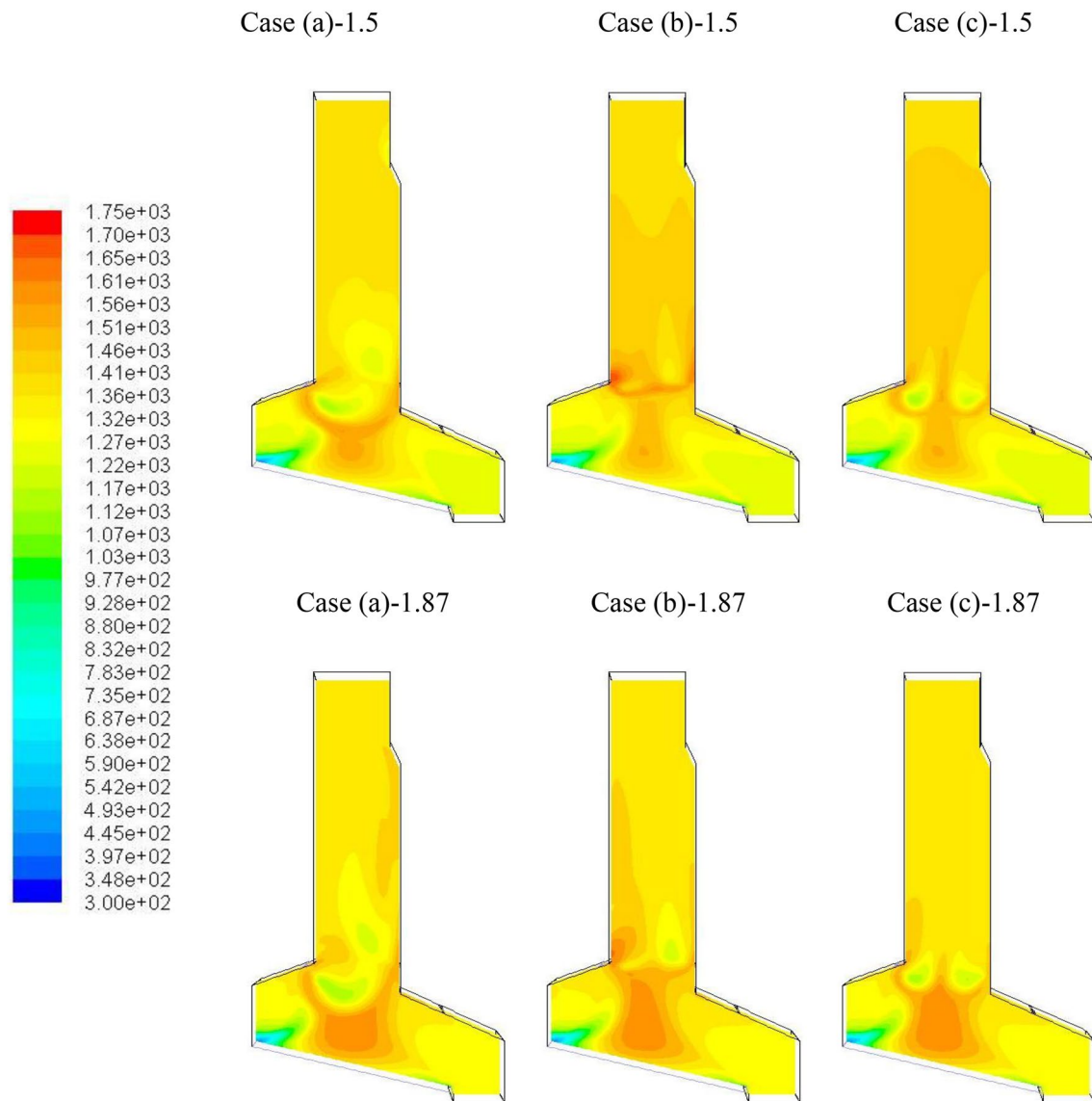


**Fig. 10** Contours of temperature in combustor for SRF-B (K)

ratio and secondary air injection angle change, the turbulent intensity on the grate is very low. Therefore, the generation of fly ash at the grate is suppressed. However, in case (a), the turbulent intensity in the main combustion chamber is lower than that in (b) and (c); thus, it is considered that the amount of fly ash that flows out from the combustion chamber to the heat exchanger is the smallest.

In Fig. 9, the velocity magnitude in the combustor increases with increasing air ratio. The velocity magnitude is the sum of the velocity vector in the x, y, and z axis directions in the 3 dimensional combustion chamber. However, it can be seen that the velocity magnitude changes in the main combustion chamber according to the secondary air injection angle. Therefore, it is possible to suppress the generation of

fly ash when the secondary air injection angles are normal to the left and right walls ( $90^\circ$ ). Also, the case of ‘Case (b)’, the secondary air injection angle are counterclockwise ( $45^\circ$ ) from normal to the left wall and normal to the right wall ( $90^\circ$ ), it can be an appropriate operating condition according to the SRFs characteristic.

#### Temperature Distribution in Combustion Chamber

The temperature distribution inside the combustion chamber with varying air ratios and secondary air injection angles is shown in Fig. 10. The overall temperature inside the combustor decreases with increasing air ratio, and the flame shape in the high temperature areas changes in accordance

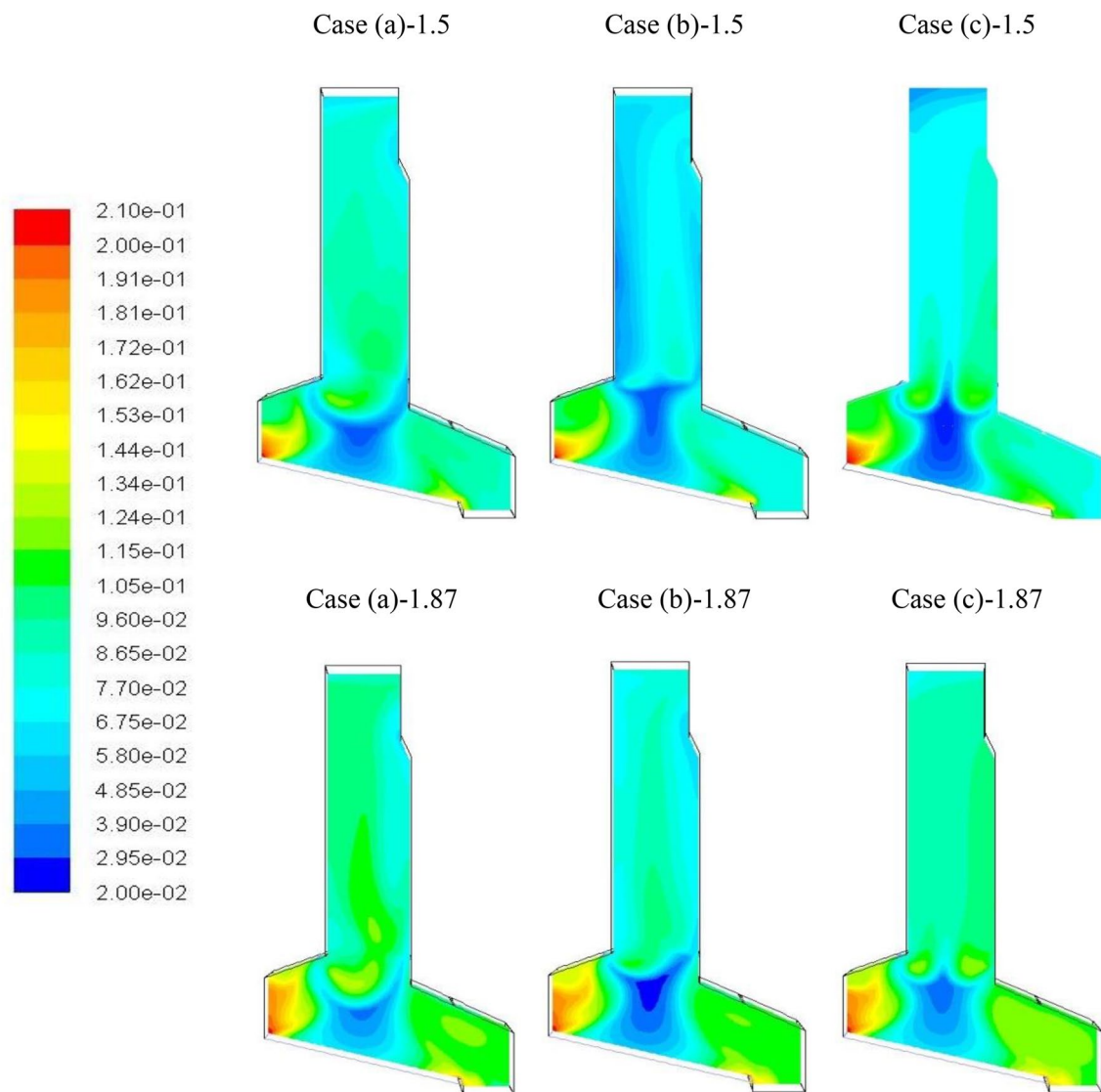


**Fig. 11** Contours of oxygen concentration in combustor for SRF-B (mole fraction)

with the secondary air injection angles. In case (a), the flame is formed in the high temperature area on the bottom surface of the grate. In case (b), the flame is partially formed in the upper part grate where the secondary air is injected, and thermal nitrogen oxide can be created by the formation of a local high temperature area. In case (c), the flame is formed in a similar manner to case (a).

#### Oxygen and Carbon Monoxide Concentration Inside Combustion Chamber

The combustion of an SRF-B can lead to the high temperature corrosion on the surface of heat recovery tube because

of the fly ash melting. The high temperature corrosion of the heat exchanger occurs by the deposition of fly ash produced by the combustion of the SRFs contained in the materials with chlorine and sulfur. Therefore, a high air ratio is required for stable waste heat recovery during SRF combustion owing to the lower temperature of flue gas. The concentration of oxygen concentration at the upper part of the grate in the combustion chamber indicates the uniform mixture of the supplied air and generated combustible gas, which is an important index for complete combustion and thermal NO<sub>x</sub> control (Fig. 11).

The concentration of CO is used as a measure for verifying incomplete combustion because CO is produced by

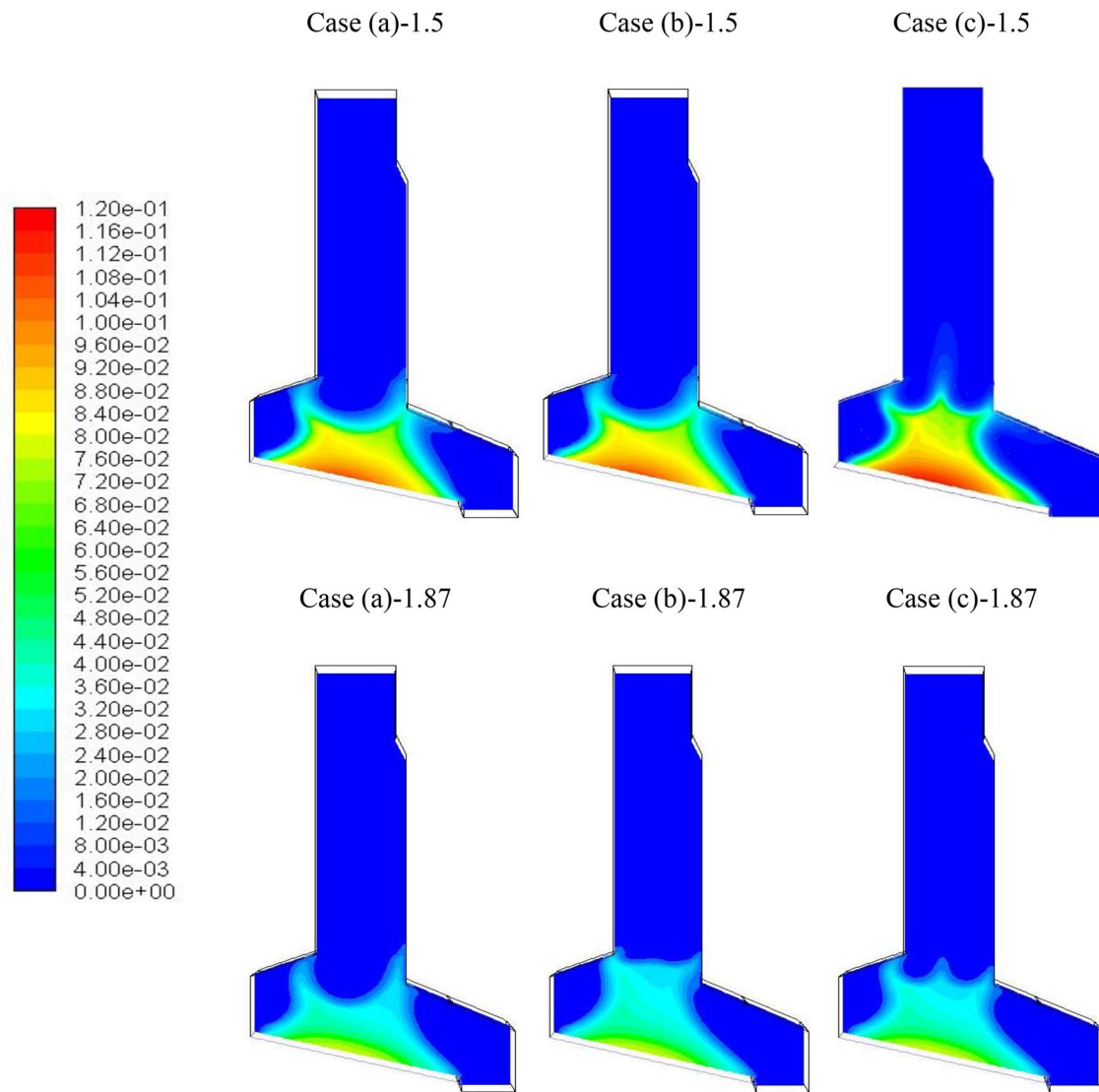


**Fig. 12** Contours of carbon monoxide concentration in combustor for SRF-B (mole fraction)

**Table 6** Temperature and mole fraction of exhaust gas at outlet of the combustion chamber

Case no.	Outlet temperature (°C)	O <sub>2</sub> (mole fraction)	CO (mole fraction)	SRF (mole fraction)
Case (a)-1.5	1063	0.0624	2.42e−05	1.30e−06
Case (b)-1.5	1076	0.0655	2.70e−05	1.42e−06
Case (c)-1.5	1103	0.0664	1.53e−04	8.98e−06
Case (a)-1.87	998	0.0864	1.18e−05	8.75e−07
Case (b)-1.87	1003	0.0931	9.54e−06	6.81e−07
Case (c)-1.87	1009	0.0921	4.77e−05	4.03e−06

insufficient oxygen in the combustion chamber (Fig. 12). The results of the numerical analysis show that the outlet temperature is the lowest in case (a)-1.87, where the air ratio is 1.87 and the secondary air injection angles are normal

to the walls (90°). However, there is no major difference compared with the results for different injection angles. In Table 6, the oxygen concentrations at the outlet of the combustion chamber are the lowest in case (a)-1.5.

## Conclusions

To develop a large-scale combustion system for power generation using SRF, which is combustible waste, we used fluff SRF, densified SRF, and two types of MSWs to produce an optimal SRF sample. The fluff SRF, densified SRF, and two types of MSWs were subjected to ultimate analysis, proximate analysis, heating value analysis, TGA and DTG. In addition, the calculation of the flow and temperature field, the chemical species concentration in the combustion chamber according to the change in air ratio and the secondary air injection angle, was calculated using computational fluid dynamics (CFD). The main conclusions are as follows:

1. The water contents of the two types of MSWs vary from 18.4 to 18.9 wt%. Ash contents are high, and volatile matter and fixed carbon contents are low. Fluff and densified SRF have large differences in their water and ash contents depending on wastes and the manufacturing method. The fuel ratios vary from 0.32–0.50 for the MSWs and 0.11–0.15 for the SRFs. The C/H ratios vary from 7.98–8.37 for the MSWs and 6.45–7.53 for the SRFs owing to high volatile matter contents with short ignition and combustion time.
2. The concentrations of Cl are 1.80 wt% and 0.12 wt% for the densified and fluff SRFs, respectively. The detected Cl concentration in the SRFs are lower than the Cl content regulation of 2.0 wt%. Additionally, the Cl component in SRF causes high temperature corrosion on the tube of heat exchangers.
3. The TGA and DTG results shows the discharge of water, volatile matter, carbon, and residual matter components, and the combustion of fixed carbon occur between reactor atmosphere temperatures of 250 °C and 500 °C for the SRFs and between 250 and 540 °C for the MSWs.
4. A large excess air ratio is required to prevent the high temperature corrosion of the heat exchangers in SRF-B combustion steam boiler. The air ratio of 1.87 used in this study is optimal for stable combustion and prevention of high temperature corrosion.

In the next step, the calculations of thermal NO<sub>x</sub> generation and simulation of the influence of design parameters, ratio of primary/secondary air and shape of wall on the secondary air injection, in commercially large-scale SRF combustion systems are needed.

**Acknowledgement** This work was supported by Korea Environment Industry & Technology Institute (KEITI) through Public Technology Program based on Environmental Policy Program, funded by Korea Ministry of Environment (MOE) (2016000710008).

## References

1. Adanez, J., Abad, A., Mendiara, T., Gayan, P., Diego, L.F., Garcia-Labiano, F.: Chemical looping combustion of solid fuels. *Prog. Energy Combust. Sci.* **65**, 6–66 (2018)
2. Iacovidou, E., Hahladakis, J., Deans, I., Velis, C., Purnell, P.: Technical properties of biomass and solid recovered fuel (SRF) co-fired with coal: impact on multi-dimensional resource recovery value. *Waste Manag.* **73**, 535–545 (2017)
3. Park, S.W., Lee, J.S., Yang, W.S., Kang, J.J., Sung, J.H., Alam, M.T., Seo, Y.C.: For waste to energy, assessment of fluff type solid refuse fuel by thermal characteristics analyses. *Procedia Environ. Sci.* **35**, 498–505 (2016)
4. Agraniotis, M., Nikolopoulos, N., Nikolopoulos, A., Grammelis, P., Kakaras, E.: Numerical investigation of solid recovered fuel's co-firing with brown coal in large scale boilers-evaluation of different co-combustion modes. *Fuel* **89**(12), 3693–3709 (2010)
5. Dunnu, G., Maier, J., Hilber, T., Scheffknecht, G.: Characterisation of large solid recovered fuel particles for direct co-firing in large PF power plants. *Fuel* **88**(12), 2403–2408 (2009)
6. Garg, A., Smith, R., Hill, D., Longhurst, P.J., Pollard, S.J.T., Simms, N.J.: An integrated appraisal of energy recovery options in the United Kingdom using solid recovered fuel derived from municipal solid waste. *Waste Manag.* **29**, 2289–2297 (2009)
7. Wu, H., Glarborg, P., Frandsen, F.J., Kim, D.J., Jensen, P.A., Sander, B.: Trace elements in co-combustion of solid recovered fuel and coal. *Fuel Process. Technol.* **105**, 212–221 (2013)
8. Arena, U., Gregorio, F.D.: Gasification of a solid recovered fuel in a pilot scale fluidized bed reactor. *Fuel* **117**, 528–536 (2014)
9. Wagland, S.T., Kilgallon, P., Coveney, R., Garg, A., Smith, R., Longhurst, P.T., Pollard, S.J.T., Simms, N.: Comparison of coal/solid recovered fuel(SRF)with coal/refuse derived fuel(RDF)in a fluidised bed reactor. *Waste Manag.* **31**, 1176–1183 (2011)
10. Bessi, C., Lombardi, L., Meoni, R., Canovai, A., Corti, A.: Solid recovered fuel: an experiment on classification and potential applications. *Waste Manag.* **47**, 184–194 (2016)
11. Gani, A., Morishita, K., Nishikawa, K., Naruse, I.: (2005) Characteristics of co-combustion of low-rank coal with biomass. *Energy Fuels* **19**(4), 1652–1659 (2005)
12. Lu, G., Yan, Y., Cornwell, S., Whitehouse, M., Riley, G.: Impact of co-firing coal and biomass on flame characteristics and stability. *Fuel* **87**, 1133–1140 (2008)
13. Molcan, P., Lu, G., Birs, L.T., Yan, Y., Taupin, B., Caillat, S.: Characterization of biomass and coal co-firing on a 3MWth combustion test facility using flame imaging and gas/ash sampling techniques. *Fuel* **88**(12), 2328–2334 (2009)
14. Sami, M., Annamalai, K., Wooldridge, M.: Co-firing of coal and biomass fuel blends. *Prog. Energy Combust. Sci.* **27**(2), 171–214 (2001)
15. Wu, H., Glarborg, P., Frandsen, F.J., Kim, D.J., Jensen, P.A., Sander, B.: Co-combustion of pulverized coal and soils recovered fuel in an entrained flow reactor-general combustion and ash behaviour. *Fuel* **90**(5), 1980–1991 (2011)
16. Vainikka, P., Bankiewicz, D., Frantsi, A., Silvennoinen, J., Hannula, J., Yrjas, P., Hupa, M.: High temperature corrosion of boiler waterwalls induced by chlorides and bromides. Part 1: occurrence of the corrosive ash forming elements in a fluidised bed boiler co-firing solid recovered fuel. *Fuel* **90**(5), 2055–2063 (2011)
17. Vainikka, P., Enestam, S., Silvennoinen, J., Taipale, R., Yrjas, P., Frantsi, A., Hannula, J., Hupa, M.: Bromine as an ash forming element in a fluidised bed boiler combusting solid recovered fuel. *Fuel* **90**(3), 1101–1112 (2011)
18. Vainio, E., Yrjas, P., Zevenhoven, M., Brink, A., Lauren, T., Hupa, M., Kajolinna, T., Vesala, H.: The fate of chlorine, sulfur, and potassium during co-combustion of bank, sludge, and solid

- recovered fuel in an industrial scale BFB boiler. *Fuel Process. Technol.* **150**(1), 59–69 (2013)
19. Ohm, T.I., Chae, J.S., Kim, Y.H., Moon, S.H.: Characteristics of fry-drying and solid refuse fuels for the organic wastes with high water content. *J. Renew. Mater. Supplement* **5**(1), 13–21 (2017)
  20. Alobaid, F., Al-Maliki, W.A.K., Lanz, T., Haaf, M.: Dynamic simulation of a municipal solid waste incinerator. *Energy* **149**, 230–249 (2018)
  21. Kim, B.J., Ryu, C.K., Lee, U.D., Kim, Y.D., Lee, J.W., Song, J.H.: A technical review on the protective measures of high temperature corrosion of heat exchangers with additives. *Clean Technol.* **23**(3), 223–236 (2017)
  22. Guessab, A., Aris, A., Bounif, A.: Simulation of turbulent piloted methane non-premixed flame based on combination of finite-rate/eddy-dissipation model. *MECHANIKA* **19**(6), 657–664 (2013)
  23. ANSYS Fluent 16.1 Users Guide, ANSYS Inc. (2015).
  24. Kim, M.S., Lee, Y.W., Park, J.J., Ryu, C.K., Ohm, T.I.: Partial oxidation of sewage sludge briquettes in a updraft fixed bed. *Waste Manag.* **49**, 202–211 (2016)
  25. Shih, T.H., Liou, W.W., Shabbir, A., Yang, Z., Zhu, J.: A new k- $\epsilon$  eddy viscosity model for high reynolds number turbulent flows. *Comput. Fluids* **24**(3), 227–238 (1995)
  26. Abdelgayed, H.M., Abdelghaffar, W.A., Shorbagy, K.E.: Flame vortex interactions in a lean premixed swirl stabilized gas turbine combustor—numerical computations. *Am. J. Sci. Ind. Res.* **4**(5), 449–467 (2013)

**Publisher's Note** Springer Nature remains neutral with regard to jurisdictional claims in published maps and institutional affiliations.